Supplement of Geosci. Model Dev., 15, 2105–2131, 2022
https://doi.org/10.5194/gmd-15-2105-2022-supplement

Geoscientific Model Development
Open Access
EGU

Supplement of

RADIv1: a non-steady-state early diagenetic model for ocean sediments in Julia and MATLAB/GNU Octave

Olivier Sulpis et al.

Correspondence to: Olivier Sulpis (o.j.t.sulpis@uu.nl)

Contents of this file

Full RADI equations

Below we detail Eq. (5) from the main text for readers interested in seeing its complete version. For solutes,

$$v_{(t+\mathrm{d}t),z} = v_{t,z} + \left[R\left(v_{t,z}\right) + - \left(u_z - \frac{d_z(v)}{\varphi_z} \cdot \frac{\mathrm{d}\varphi_z}{\mathrm{d}z} - d°(v) \cdot \frac{\mathrm{d}\left(1/\theta_z{}^2\right)}{\mathrm{d}z} \right) \cdot \frac{v_{(z+\mathrm{d}z)} - v_{(z-\mathrm{d}z)}}{2\mathrm{d}z} + d_z(v) \cdot \frac{v_{(z-dz)} - 2v_z + v_{(z+dz)}}{(dz)^2} + \alpha_z(v_w - v_z) \right] \cdot dt$$

and for solids,

$$v_{(t+\mathrm{d}t),z} = v_{t,z} + \left[R\left(v_{t,z}\right) + - \left(w_z - \frac{\mathrm{d}b_z}{\mathrm{d}z} - \frac{b_z}{\varphi_{s,z}} \cdot \frac{\mathrm{d}\varphi_{s,z}}{\mathrm{d}z} \right) \cdot \frac{(1-\sigma_z)v_{(z+dz)} + 2\sigma_z v_z - (1+\sigma_z)v_{(z-dz)}}{2dz} + d_z(v) \cdot \frac{v_{(z-dz)} - 2v_z + v_{(z+dz)}}{(dz)^2} \right] \cdot dt$$

Using TAlk and ΣCO_2 as solute variables, rather than their individual components

Transport-reaction modelling of the carbonate system is challenging, and trade-offs must be made (e.g., Boudreau, 1997; Hoffmann et al., 2008). Modelling the carbonate system in the water column normally involves transport of total alkalinity and total dissolved inorganic carbon because these model variables are conservative (Humphreys et al., 2018), and both are transported with the water (i.e., differences in molecular diffusion among the species involved do not matter in advection dominated systems). In non-permeable sediments, molecular diffusion dominates transport and species diffuse according to their own gradient (e.g., the gradient of carbon dioxide may differ from that of the carbonate ion). Moreover, species may have different diffusion coefficients. Consequently, a more accurate way to represent the carbonate system in non-permeable sediments is to have transport-reaction equations for all species involved (e.g., protons, bicarbonate, carbonate, carbon dioxide). The most accurate way would be to include also changes in complex formation and electroneutrality constraints (Boudreau et al., 2004).

However, this gain in model accuracy comes at the expense of model complexity and computational demand, while the uncertainty due to lumping carbonic acid, bicarbonate and carbonate transport is usually less than other uncertainties related to thermodynamic constants needed in the calculation and tortuosity corrections for diffusion coefficients. Most of the uncertainty surrounding $CaCO_3$ saturation state estimates stems from the large uncertainty within the $CaCO_3$ equilibrium constants rather than that associated with carbonate ion (Orr et al., 2018; Sulpis et al., 2020); this uncertainty is independent of the transport modelling approach used.

HCO_3^- is the dominant dissolved inorganic carbon species at pH values typical of porewaters, see Fig. S2. In Fig. S2, we show what the diffusion of DIC would be if it was computed as a weighted arithmetic average of the diffusion coefficients of each of the DIC components. At pH ~7, the 'true' DIC diffusion coefficient (the weighted arithmetic average) is about 4% higher than the diffusion coefficient of HCO_3^- alone. That gap becomes negligible at higher pH. Thus, using the HCO_3^- diffusion coefficient as a surrogate for that of TAlk and DIC, as it has been done by other, similar models, such as that of Kanzaki et al. (2021), should be acceptable if the pH is not too low.

Table S1. Environmental conditions, bottom-water and sediment properties for the North-western Atlantic Ocean station.

Variable	Value	Source
Station ID	Station #9	Hales et al. (1994)
Location	North Atlantic	Hales et al. (1994)
Coordinates	34.33N / 70.35W	Hales et al. (1994)
Depth	5210 m	Hales et al. (1994)
Temperature	2.2 °C	Hales et al. (1994)
Salinity	34.9	Hales et al. (1994)
DBL thickness	938 µm	Sulpis et al. (2018)
Solid fluxes to the seafloor (mol m^{-2} a^{-1})		
POC flux (F_{POC})	0.18 (6.0 g POM m^2 a^{-1})	Hales et al. (1994)
Fast-decay POC	0.70 x F_{POC}	Assumed
Slow-decay POC	0.27 x F_{POC}	Assumed
Refractory POC	0.03 x F_{POC}	Assumed
$CaCO_3$ flux (F_{CaCO3})	0.20 (20.02 g $CaCO_3$ m^{-2} a^{-1})	Hales et al. (1994)
Calcite	F_{CaCO3}	Assumed
Aragonite	0	Assumed
MnO_2 flux (F_{MnO2})	0.0005	Assumed
$Fe(OH)_3$ flux ($F_{Fe(OH)3}$)	0.0005	Assumed
FeS flux (F_{FeS})	0	Boudreau (1996)
Sediment surface properties		
Surface [$CaCO_3$]	27 dry wt %	Hales et al. (1994)
Surface [POC]	0.31 dry wt %	Hales et al. (1994)
Clay flux	26 g m^{-2} a^{-1}	Assumed
Surface porosity	0.91	Assumed
Porosity at depth	0.74	Assumed
Bottom-water chemistry		
TAlk	2342 µmol kg^{-1}	Hales et al. (1994)
ΣCO_2	2186 µmol kg^{-1}	Hales et al. (1994)
$[O_2]$	266.6 µmol kg^{-1}	Hales et al. (1994)
$[\Sigma NO_3]$	20.0668 µmol kg^{-1}	GLODAPv2 (Lauvset et al., 2016)
$[\Sigma SO_4]$	29.180 mmol kg^{-1}	Computed from S (Millero, 2013)
$[\Sigma PO_4]$	1.3561 µmol kg^{-1}	GLODAPv2 (Lauvset et al., 2016)
$[\Sigma NH_4]$	0	Assumed
$[\Sigma H_2S]$	0	Assumed
$[Mn^{2+}]$	0.5 nmol kg^{-1}	Typical deep-sea value (Morton et al., 2019)
$[Fe^{2+}]$	0.5 nmol kg^{-1}	Typical deep-sea value (Abadie et al., 2017)
$[Ca^{2+}]$	10.255 mmol kg^{-1}	Computed from S (Riley and Tongudai, 1967)
$[CO_3^{2-}]_{SW}$ (µmol kg^{-1})	102.6 µmol kg^{-1}	Computed (RADI)
$[CO_3^{2-}]_{eq\ Calcite}$ (µmol kg^{-1})	117.6 µmol kg^{-1}	Computed (RADI)
$[CO_3^{2-}]_{eq\ Arag.}$ (µmol kg^{-1})	175.5 µmol kg^{-1}	Computed (RADI)
Ω_{ca}	0.88	Computed (RADI)
Ω_{ar}	0.59	Computed (RADI)

Table S2. Environmental conditions, bottom-water and sediment properties for the Southern Pacific station.

Variable	Value	Source
Station ID	Station #7.3	Sayles et al. (2001)
Location	Southern Pacific	Sayles et al. (2001)
Coordinates	60.15S / 170.11W	Sayles et al. (2001)
Depth	3860 m	Sayles et al. (2001)
Temperature	0.84 °C	Sayles et al. (2001)
Salinity	34.696	Sayles et al. (2001)
DBL thickness	715 µm	Sulpis et al. (2018)
Solid fluxes to the seafloor (mol m^{-2} a^{-1})		
POC flux (F_{POC})	0.138 (4.6 g POM m^2 a^{-1})	Assumed
Fast-decay POC	0.70 x F_{POC}	Assumed
Slow-decay POC	0.27 x F_{POC}	Assumed
Refractory POC	0.03 x F_{POC}	Assumed
$CaCO_3$ flux (F_{CaCO3})	0.25 (25.02 g $CaCO_3$ m^{-2} a^{-1})	Assumed
Calcite	F_{CaCO3}	Assumed
Aragonite	0	Assumed
MnO_2 flux (F_{MnO2})	0.0005	Assumed
$Fe(OH)_3$ flux ($F_{Fe(OH)3}$)	0.0005	Assumed
FeS flux (F_{FeS})	0	Boudreau (1996)
Sediment surface properties		
Surface [$CaCO_3$]	37.7 dry wt %	Sayles et al. (2001)
Surface [POC]	0.37 dry wt %	Sayles et al. (2001)
Clay flux	32 g m^{-2} a^{-1}	Sayles et al. (2001), November – February average
Surface porosity	0.91	Sayles et al. (2001)
Porosity at depth	0.87	Assumed
Bottom-water chemistry		
TAlk	2365 µmol kg^{-1}	GLODAPv2 (Lauvset et al., 2016)
ΣCO_2	2260 µmol kg^{-1}	GLODAPv2 (Lauvset et al., 2016)
[O_2]	215.7 µmol kg^{-1}	GLODAPv2 (Lauvset et al., 2016)
[ΣNO_3]	32.2416 µmol kg^{-1}	GLODAPv2 (Lauvset et al., 2016)
[ΣSO_4]	29.010 mmol kg^{-1}	Computed from S (Millero, 2013)
[ΣPO_4]	2.2428 µmol kg^{-1}	GLODAPv2 (Lauvset et al., 2016)
[ΣNH_4]	0	Assumed
[ΣH_2S]	0	Assumed
[Mn^{2+}]	0.5 nmol kg^{-1}	Typical deep-sea value (Morton et al., 2019)
[Fe^{2+}]	0.5 nmol kg^{-1}	Typical deep-sea value (Abadie et al., 2017)
[Ca^{2+}]	10.196 mmol kg^{-1}	Computed from S (Riley and Tongudai, 1967)
$[CO_3^{2-}]_{SW}$ (µmol kg^{-1})	77.5 µmol kg^{-1}	Computed (RADI)
$[CO_3^{2-}]_{eq\ Calcite}$ (µmol kg^{-1})	91.7 µmol kg^{-1}	Computed (RADI)
$[CO_3^{2-}]_{eq\ Arag.}$ (µmol kg^{-1})	138.9 µmol kg^{-1}	Computed (RADI)
Ω_{ca}	0.85	Computed (RADI)
Ω_{ar}	0.56	Computed (RADI)

Table S3. Environmental conditions, bottom-water and sediment properties for the Central Equatorial Pacific station.

Variable	Value	Source
Station ID	Station #W-2	Berelson et al. (1994) / Hammond et al. (1996)
Location	Equatorial Pacific	Berelson et al. (1994) / Hammond et al. (1996)
Coordinates	0.0N / 139.9W	Berelson et al. (1994) / Hammond et al. (1996)
Depth	4370 m	Berelson et al. (1994) / Hammond et al. (1996)
Temperature	1.4 °C	GLODAPv2 (Lauvset et al., 2016)
Salinity	34.69	GLODAPv2 (Lauvset et al., 2016)
DBL thickness	1 mm	Assumed
Solid fluxes to the seafloor (mol m^{-2} a^{-1})		
POC flux (F_{POC})	0.20 (6.6 g POM m^{2} a^{-1})	Assumed
Fast-decay POC	0.70 x F_{POC}	Assumed
Slow-decay POC	0.27 x F_{POC}	Assumed
Refractory POC	0.03 x F_{POC}	Assumed
$CaCO_3$ flux (F_{CaCO3})	0.22 (22.02 g $CaCO_3$ m^{-2} a^{-1})	Assumed
Calcite	F_{CaCO3}	Assumed
Aragonite	0	Assumed
MnO_2 flux (F_{MnO2})	0.0005	Assumed
$Fe(OH)_3$ flux ($F_{Fe(OH)3}$)	0.0005	Assumed
FeS flux (F_{FeS})	0	Boudreau (1996)
Sediment surface properties		
Surface [$CaCO_3$]	76.1 dry wt %	Hammond et al (1996) Table 1
Surface [POC]	0.24 dry wt %	Hammond et al (1996) Table 1
Clay flux	2 g m^{-2} a^{-1}	Hammond et al (1996)
Surface porosity	0.85	Hammond et al (1996)
Porosity at depth	0.74 (4cm)	Berelson et al. (1994)
Bottom-water chemistry		
TAlk	2426.0 µmol kg^{-1}	GLODAPv2 (Lauvset et al., 2016)
ΣCO_2	2324.3 µmol kg^{-1}	GLODAPv2 (Lauvset et al., 2016)
[O_2]	159.7 µmol kg^{-1}	GLODAPv2 (Lauvset et al., 2016)
[ΣNO_3]	36.93 µmol kg^{-1}	GLODAPv2 (Lauvset et al., 2016)
[ΣSO_4]	29.005 mmol kg^{-1}	Computed from S (Millero, 2013)
[ΣPO_4]	2.39 µmol kg^{-1}	GLODAPv2 (Lauvset et al., 2016)
[ΣNH_4]	0	Assumed
[ΣH_2S]	0	Assumed
[Mn^{2+}]	0.5 nmol kg^{-1}	Typical deep-sea value (Morton et al., 2019)
[Fe^{2+}]	0.5 nmol kg^{-1}	Typical deep-sea value (Abadie et al., 2017)
[Ca^{2+}]	10.193 mmol kg^{-1}	Computed from S (Riley and Tongudai, 1967)
$[CO_3^{2-}]_{SW}$ (µmol kg^{-1})	77.9 µmol kg^{-1}	Computed (RADI)
$[CO_3^{2-}]_{eq\ Calcite}$ (µmol kg^{-1})	100.0 µmol kg^{-1}	Computed (RADI)
$[CO_3^{2-}]_{eq\ Arag.}$ (µmol kg^{-1})	150.7 µmol kg^{-1}	Computed (RADI)
Ω_{ca}	0.78	Computed (RADI)
Ω_{ar}	0.52	Computed (RADI)

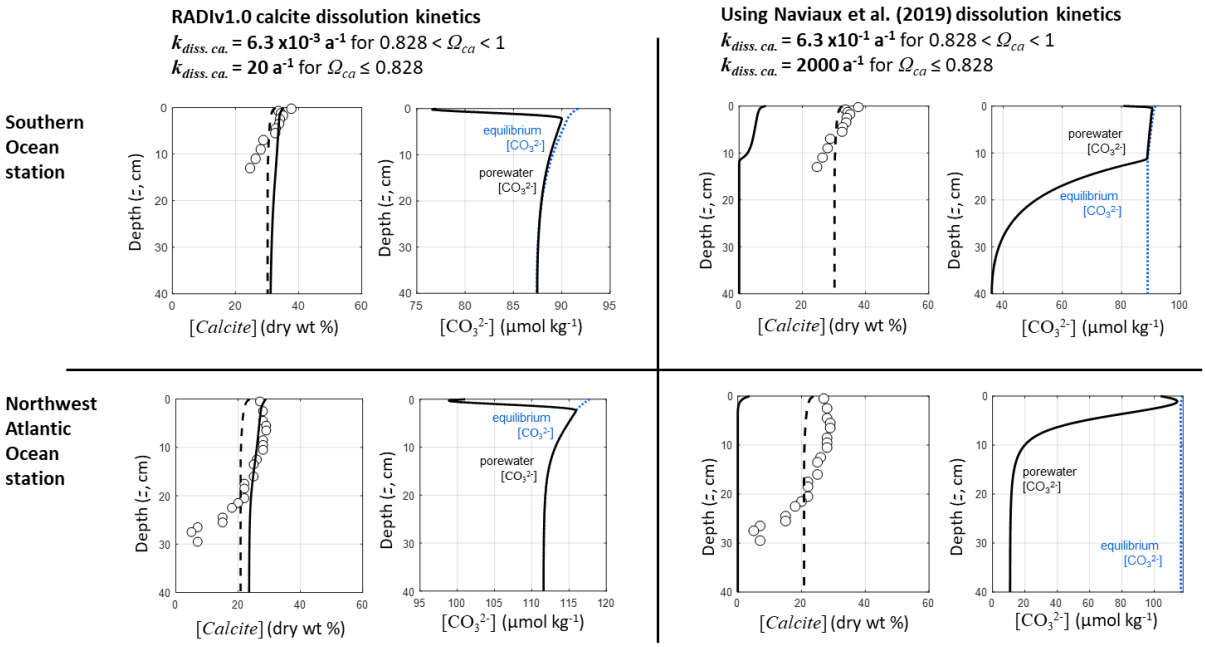

Figure S1. *Comparison of predicted calcite and CO_3^{2-} concentration profiles using the calcite dissolution kinetics implemented in RADIv1 (left) and using the rate constants from the original publication (Naviaux et al., 2019a) coupled with the surface area of foraminifera (400 m^2 mol^{-1}, from Subhas et al., 2018). The dashed line represents results from the MUDS model.*

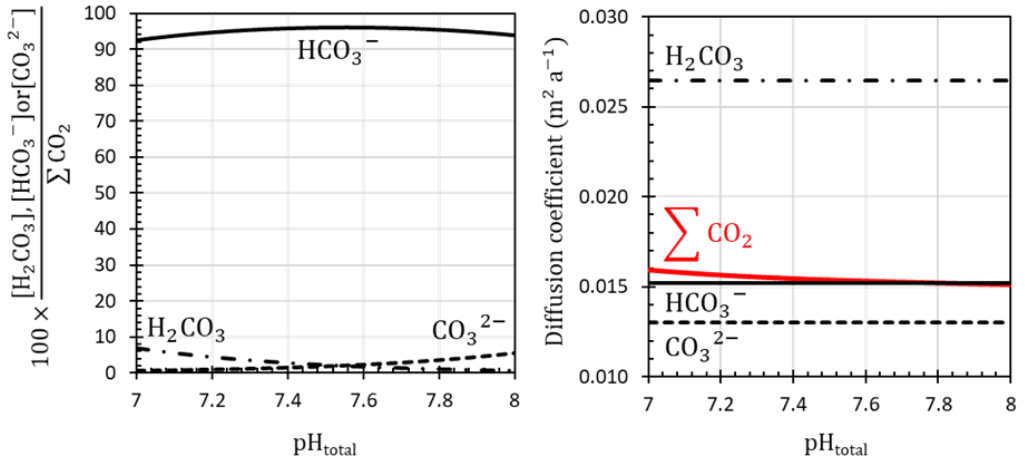

Figure S2. *(left) Relative proportion of each of the three species constituting ΣCO_2 as a function of seawater pH, expressed on the total scale. (right) Diffusion coefficients of each of the three species constituting ΣCO_2, as well as of ΣCO_2 itself when computed as an weighted arithmetic average of the diffusion coefficients of each of its constituting species, as a function of seawater pH expressed on the total scale.*

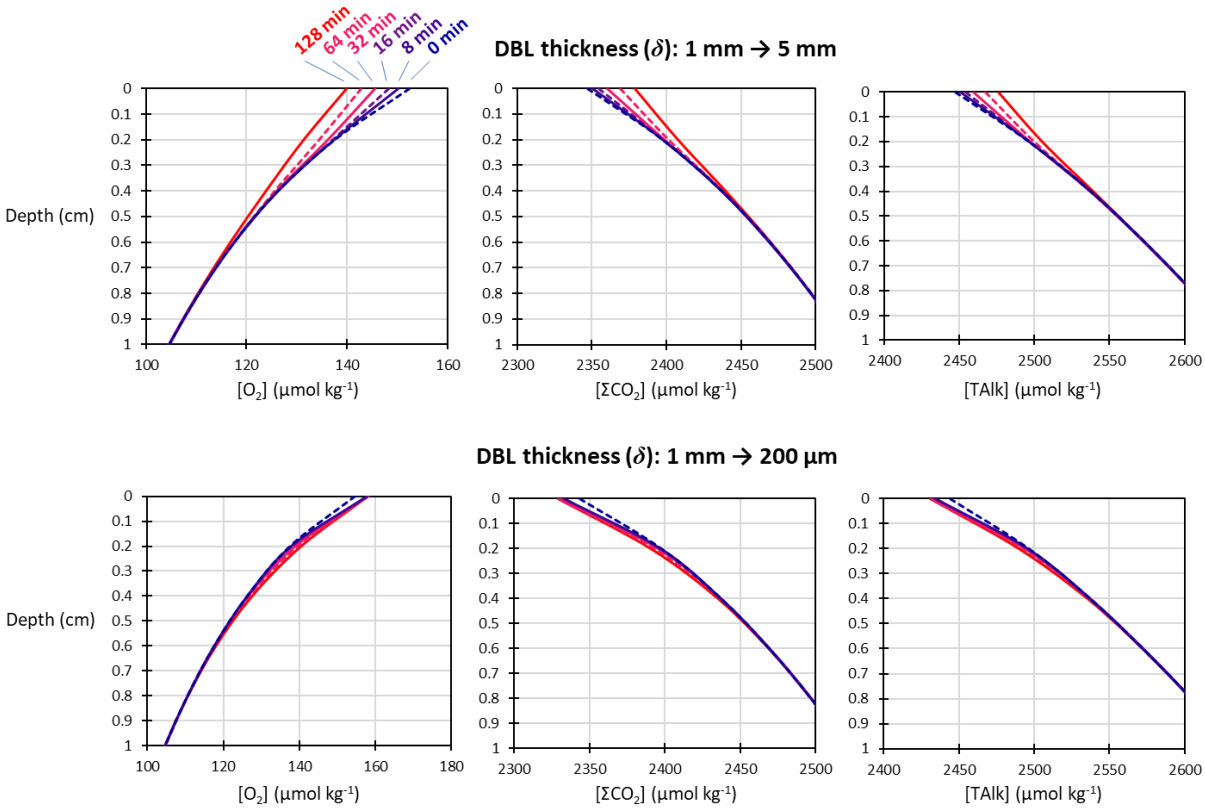

Figure S3. *Porewater* $[O_2]$, ΣCO_2 *and* TAlk *depth profiles as a function of time following an instantaneous change in the diffusive boundary layer thickness (δ).*

Supplementary references

Abadie, C., Lacan, F., Radic, A., Pradoux, C. and Poitrasson, F. (2017) Iron isotopes reveal distinct dissolved iron sources and pathways in the intermediate versus deep Southern Ocean. Proceedings of the National Academy of Sciences 114, 858-863.

Berelson, W.M., Hammond, D.E., McManus, J. and Kilgore, T.E. (1994) Dissolution kinetics of calcium carbonate in equatorial Pacific sediments. Global Biogeochemical Cycles 8, 219-235.

Boudreau, B.P. (1996) A method-of-lines code for carbon and nutrient diagenesis in aquatic sediments. Computers & Geosciences 22, 479-496.

Boudreau, B.P. (1997) Diagenetic Models and Their Implementation. Springer-Verlag, Berlin, 414 pp. 1997

Boudreau, B.P., Meysman, F.J.R., Middelburg, J.J. (2004) Multicomponent ionic diffusion in porewaters: Coulombic effects revisited. Earth and Planetary Science Letters, 222, 653-666.

Hales, B., Emerson, S. and Archer, D. (1994) Respiration and dissolution in the sediments of the western North Atlantic: estimates from models of in situ microelectrode measurements of porewater oxygen and pH. Deep Sea Research Part I: Oceanographic Research Papers 41, 695-719.

Hammond, D.E., McManus, J., Berelson, W.M., Kilgore, T.E. and Pope, R.H. (1996) Early diagenesis of organic material in equatorial Pacific sediments: stpichiometry and kinetics. Deep Sea Research Part II: Topical Studies in Oceanography 43, 1365-1412.

Hofmann, A.F., Meysman, F.J.R., Soetaert, K., Middelburg, J.J. (2008) A step-by-step procedure for pH model construction in aquatic systems. Biogeosciences 5, 227-251.

Humphreys, M.P., Daniels, C.J., Wolf-Gladrow, D.A., Tyrrell, T., Achterberg, E.P. (2018) On the influence of marine biogeochemical processes over CO_2 exchange between the atmosphere and ocean. Marine Chemistry, 199, 1-11.

Kanzaki, Y., Hülse, D., Turner, S.K., Ridgwell, A. (2021) A model for marine sedimentary carbonate diagenesis and paleoclimate proxy signal tracking: IMP v1.0. Geoscientific Model Development, 14, 5999-6023.

Lauvset, S.K., Key, R.M., Olsen, A., van Heuven, S., Velo, A., Lin, X., Schirnick, C., Kozyr, A., Tanhua, T., Hoppema, M., Jutterström, S., Steinfeldt, R., Jeansson, E., Ishii, M., Perez, F.F., Suzuki, T. and Watelet, S. (2016) A new global interior ocean mapped climatology: the 1° × 1° GLODAP version 2. Earth System Science Data 8, 325-340.

Millero, F.J. (2013) Chemical Oceanography, Fourth Edition. CRC Press - Taylor & Francis Group, Boca Raton.

Morton, P.L., Landing, W.M., Shiller, A.M., Moody, A., Kelly, T.D., Bizimis, M., Donat, J.R., De Carlo, E.H. and Shacat, J. (2019) Shelf Inputs and Lateral Transport of Mn, Co, and Ce in the Western North Pacific Ocean. Frontiers in Marine Science 6.

Naviaux, J.D., Subhas, A.V., Dong, S., Rollins, N.E., Liu, X., Byrne, R.H., Berelson, W.M. and Adkins, J.F. (2019a) Calcite dissolution rates in seawater: Lab vs. in-situ measurements and inhibition by organic matter. Marine Chemistry 215.

Orr, J. C., Epitalon, J.-M., Dickson, A. G., and Gattuso, J.-P. (2018) Routine uncertainty propagation for the marine carbon dioxide system, Mar. Chem., 207, 84–107.

Riley, J.P. and Tongudai, M. (1967) The major cation/chlorinity ratios in sea water. Chemical Geology 2, 263-269.

Sayles, F.L., Martin, W.R., Chase, Z. and Anderson, R.F. (2001) Benthic remineralization and burial of biogenic SiO_2, $CaCO_3$, organic carbon, and detrital material in the Southern Ocean along a transect at 170 West. Deep Sea Research II 48, 4323-4383.

Subhas, A.V., Rollins, N.E., Berelson, W.M., Erez, J., Ziveri, P., Langer, G. and Adkins, J.F. (2018) The dissolution behavior of biogenic calcites in seawater and a possible role for magnesium and organic carbon. Marine Chemistry 205, 100-112.

Sulpis, O., Boudreau, B.P., Mucci, A., Jenkins, C.J., Trossman, D.S., Arbic, B.K. and Key, R.M. (2018) Current $CaCO_3$ dissolution at the seafloor caused by anthropogenic CO_2. Proceedings of the National Academy of Sciences 115, 11700-11705.

Sulpis, O., Lauvset, S.K., Hagens, M. (2020) Current estimates of K_1* and K_2* appear inconsistent with measured CO2 system parameters in cold oceanic regions. Ocean Science 16(4), 847-862.